Journal of Microbiological Methods 178 (2020) 106071

Contents lists available at ScienceDirect

Journal of Microbiological Methods

journal homepage: www.elsevier.com/locate/jmicmeth

# Rapid and dynamic detection of antimicrobial treatment response using spectral amplitude modulation in MZO nanostructure-modified quartz crystal microbalance

Yifan Wu[a], Guangyuan Li[a], Yuzhi Hong[b], Xilin Zhao[b], Pavel Ivanoff Reyes[a,*], Yicheng Lu[a,*]

[a] Department of Electrical and Computer Engineering, Rutgers University, Piscataway, NJ 08854-8058, USA
[b] Public Health Research Institute, Department of Microbiology, Biochemistry & Molecular Genetics, New Jersey Medical School, Rutgers University, Newark, NJ 07103-3535, USA

ARTICLE INFO

*Keywords:*
Magnesium zinc oxide nanostructures
Bulk acoustic wave sensors
Quartz crystal microbalance
Antimicrobial susceptibility
Bacterial culture monitoring

ABSTRACT

We report a dynamic and rapid detection of the response of *S. epidermidis* to various antimicrobial treatments utilizing the real-time spectral amplitude modulations of the magnesium zinc oxide nanostructure-modified quartz crystal microbalance ($MZO_{nano}$-QCM) biosensor. The sensor consists of a quartz crystal microbalance (QCM) with magnesium zinc oxide (MZO) nanostructures grown directly on the sensing electrode using metal-organic chemical vapor deposition (MOCVD). Combining the high sensitivity detection of bacteria provided by the MZO nanostructures with the QCM's dynamic acoustic spectrum makes a highly-sensitive dynamic biosensor well-suited for monitoring viscoelastic transitions during drug treatment compared to the QCM's conventional frequency shift signals. We demonstrated dynamically monitoring the response of *S. epidermidis* to various concentrations of the drug ciprofloxacin, and response to three different antimicrobials vancomycin, oxacillin, and ciprofloxacin, using spectral amplitude modulations of the $MZO_{nano}$-QCM. Our results indicate that the amplitude modulations exhibit high sensitivity to *S. epidermidis* response to different drug treatments compared to the conventional frequency shift signals of the device, allowing for rapid determination (within 1.5 h) of the efficacy of the antimicrobial drug. The high sensitivity demonstrated by the spectral amplitude modulations is attributed to the direct relationship of these signals to the viscoelastic transitions of the bacterial cells on the device's sensing area while responding to drug treatment. This relationship is established by the Butterworth-Van-Dyke (BVD) model of the $MZO_{nano}$-QCM. Standard microbiological protocols and assays were performed to determine the optimal drug dosages and the minimum inhibitory concentrations to serve as the benchmark for the sensor data.

## 1. Introduction

Antimicrobial drugs have greatly reduced infection-related illnesses and mortality. However, the extended use of antibiotics causes microorganisms to become adapted to these drugs through genetic alterations thus giving rise to antimicrobial resistance (AMR). AMR is threatening to become the next pandemic and is being considered a major global health concern by the US Centers for Disease Control (CDC) (U.S. CDC, 2013). However, the currently available conventional laboratory methods to determine antimicrobial susceptibility rely on labor-intensive and time-consuming assays and methodologies (Khan et al., 2019). These currently available laboratory methods include bacterial colony counting on agar plates, drug susceptibility from broth dilution protocols, disk diffusion (Jorgensen and Turnidge, 2015), including E-Test agar strips and optical methods such as the Klett-Summerson turbidity colorimetry (Min et al., 1984) and optical density (OD) absorption spectrum techniques (Domingues et al., 2001). Several more advanced spectroscopic techniques have also emerged such as the surface plasmon resonance spectroscopy (SPR) and surface-enhanced Raman scattering (SERS) spectroscopy that have been utilized for rapid determination of drug susceptibility or resistance (Syal et al., 2016; Chabot et al., 2009) however, these tests require invasive tagging of certain molecules contained in the bacterial cells. Moreover, these spectroscopic methods require complex and costly equipment that are not likely to be adopted easily for routine clinical laboratory uses. There is therefore a need for simple, cost-effective, dynamic, highly sensitive detection methods for determining antimicrobial susceptibility and resistance.

* Corresponding authors.
*E-mail addresses:* pavelrey@scarletmail.rutgers.edu (P.I. Reyes), ylu@soe.rutgers.edu (Y. Lu).

https://doi.org/10.1016/j.mimet.2020.106071
Received 4 May 2020; Received in revised form 27 September 2020; Accepted 29 September 2020
Available online 02 October 2020

MZO belongs to the oxide semiconductor family of materials under the zinc oxide (ZnO) category. Zinc oxide and MZO by extension is the 5th most abundant material on earth, and is emerging as a competitive alternative to silicon as a semiconductor material for microelectronic devices. With proper doping, ZnO and its nanostructures can be made into a multifunctional material that is particularly useful for sensing applications such as semiconductivity (Srikant et al., 1995), piezoelectricity (Onodera et al., 1997), surface morphology tuning (Reyes et al., 2013), wettability control (Zhang et al., 2007), and sensitivity to various chemical and biological substances (Anisimkin et al., 1995; Hsueh et al., 2007; Wei et al., 2006). MZO can be formed by doping a small percentage of Mg into ZnO. MZO essentially possesses all the properties of ZnO, while having additional advantages of thermal stability (Ku et al., 2011) and large range of pH tolerance during device fabrication (Hupkes et al., 2012) and bio-testing process (Reyes et al., 2017) in comparison with the pure ZnO. These abovementioned properties of MZO make it a highly viable material biointerface for biosensing devices. These MZO-based biointerface materials enable high sensitivity through nanostructured surface morphology that provides very large effective sensing area. MZO nanostructures also provide controllable surface wettability, which significantly increases sample intake (cell capture number), and material stability due to its tolerance to a large range of pH values of solutions.

Bulk acoustic wave (BAW) devices are typically comprised of piezoelectric thin films as the active component which is sandwiched between two conducting electrodes. Voltage signals applied across the electrodes cause longitudinal acoustic wave resonances along the bulk of the piezoelectric material making the device an efficient resonator. These BAW resonators have advantages as a microelectronic device such as small size, low insertion loss, and lower power consumption. The quartz crystal microbalance (QCM) is a popular BAW device that has a high quality (Q) factor, typically $10^4$ to $10^5$ at room temperature (Rodahl et al., 1995). The QCM can operate in the range of several MHz to tens of MHz and have been used primarily for mass detection. QCM sensors have also been used in biological applications such as detection of biochemical receptor binding (Atay et al., 2016; Pirinçci et al., 2018). The QCM combined with ZnO nanostructures were demonstrated to perform the detection of DNA immobilization (Reyes et al., 2009), and biological cell monitoring and adhesion (Alessandrini et al., 2006; Lee et al., 2008).

There had been a number of reports utilizing the QCM for the purposes of sensing bacterial cells. In some reports the QCM sensing electrode was coated with biochemically-functionalized layers that are conjugate pairs to the target bacterial cells directly or indirectly through their extracellular secretions. These functionalized layers consisted of monoclonal antibodies (Haob et al., 2009; Kleo et al., 2012; Park et al., 2000), DNA oligonucleotides and proteins (Kon et al., 2007, 2011). Other works demonstrated detection of bacterial cells through a QCM coated with self-assembled monolayers (Cheng et al., 2014; Su and Li, 2004) or with nanoparticles (Kurosawa et al., 2006; Liu et al., 2007; Mao et al., 2006) to increase the sensitivity of the QCM by increasing the effective sensing surface area. These self-assembled monolayers and nanoparticles were functionalized with receptor biomolecules for the target cell membranes or their extracellular secretions. The mechanism of detection for all these reports is the change in operational frequency of the QCM as it experiences increase in mass on its sensing surface. Our research group has previously demonstrated QCM-based sensors with high sensitivities to mass accumulation of mammalian cell and bacterial cell growth through large frequency shifts by integrating ZnO and MZO nanostructures on the sensing electrode of the QCM (Reyes et al., 2013, 2017).

In this paper we combine the enhanced sensing capability of the MZO nanostructures with the dynamic and real time capability of the QCM device to form the $MZO_{nano}$-QCM biosensor. The $MZO_{nano}$-QCM is comprised of a quartz crystal microbalance (QCM) device with its active sensing electrode coated with magnesium zinc oxide (MZO) nanostructures. We aim to demonstrate the dynamic real-time monitoring of culture growth and antimicrobial treatment effects on the Gram-positive strain *Staphylococcus epidermidis* (*S. epidermidis*) using the $MZO_{nano}$-QCM for various antibiotics (ciprofloxacin, oxacillin, and vancomycin) treatments, as well as dynamically monitoring the effects of dosage-dependent ciprofloxacin treatments. Traditionally the mechanism of detection for QCM-based sensors is mass accumulation on the sensing electrode as manifested by the shift in resonant frequency. However, in this paper in addition to using the frequency shift mechanism we aim to utilize the motional resistance, a parameter we derived from the dynamic spectral amplitude modulations of the acoustic wave signals of the $MZO_{nano}$-QCM. We will compare the capabilities of both sensing mechanisms of the biosensors and postulate that the motional resistance parameter would deliver more accuracy, rapidity and sensitivity in real-time detection of the transitory behavior of the bacterial strains under study, during normal growth and dosage dependent drug treatments.

## 2. Materials and methods

### 2.1. Fabrication of the $MZO_{nano}$-QCM

The $MZO_{nano}$-QCM sensor was fabricated by integrating MZO nanostructures with the QCM. Fig. 1(a–b) shows the device structure of the biosensor. The top and bottom electrodes of the QCM consist of Au thin films, each of which has a thickness of 100 nm. The piezoelectric layer is made of AT-cut quartz with a thickness of 166.6 μm. The QCM diameter is 1.37 cm with the sensing area of 0.205 $cm^2$. The MZO nanostructures were grown directly on the top electrode using metalorganic chemical vapor deposition (MOCVD) using Diethylzinc (DEZn) as the Zn source, $MCp_2Mg$ (bis-(methyl-cyclopentadienyl) magnesium) as the Mg source, and ultra-high purity (99.999%) oxygen gas as the oxidizer. The field effect scanning electron microscope (FESEM) image of the MOCVD-grown MZO nanostructures is shown in Fig. 1(c) showing uniform nanorods averaging 405 nm in height. During the MOCVD deposition, a small percentage amount of Mg is introduced into the ZnO source to form the MZO films. The substrate temperature was set to 500 °C to attain the nanostructure morphology of the MZO film on the QCM's top electrode. The nanostructure surface morphology of MZO grown on the QCM top electrode dramatically increases the effective surface area available for sensing. Pure ZnO is known to release $Zn^{2+}$ in cell growth solutions which could be toxic to the cell culture (Hupkes et al., 2012). The introduction of Mg to form MZO stabilizes the Zn binding in the nanostructure material. Using MZO instead of pure ZnO as the sensor coating material decreases the $Zn^{2+}$ concentration in the cell medium by four-fold compared to the pure ZnO, lowering the toxicity of the sensor with the cell culture and prevents etching of the MZO film by acidic media (Reyes et al., 2017; Hupkes et al., 2012).

The operating frequencies of the standard QCM, and $MZO_{nano}$-QCM were measured to be 10 MHz, and 9.912 MHz, respectively. All devices were sterilized and deployed inside a Teflon cell-growth wells and seeded with the bacterial cells. These were in turn placed inside a standard $CO_2$ incubator under controlled temperature at 37° C. The sensors were characterized using an HP 8573D Network Analyzer (Agilent Technologies, Palo Alto, CA), which were connected via IEEE-488 general purpose interface bus (GPIB) to the universal serial bus (USB) of a microprocessor running an automatic control and data acquisition program. The acoustic wave transmission spectrum ($Z_{21}(\omega)$) of the device was automatically measured at fixed time intervals and digitally stored for a fixed monitoring interval during the microbial culture growth on the sensors inside the incubator. The output of the sensor devices was in the form of time-frequency set of signals. These signals were then analyzed by extracting the peak frequency shifts ($\Delta f$), and motional resistance ($R_{Load}(\omega)$) from the spectral amplitude modulations experienced by the devices relative to their starting frequencies and amplitudes due to the mass change and viscoelastic transitions on

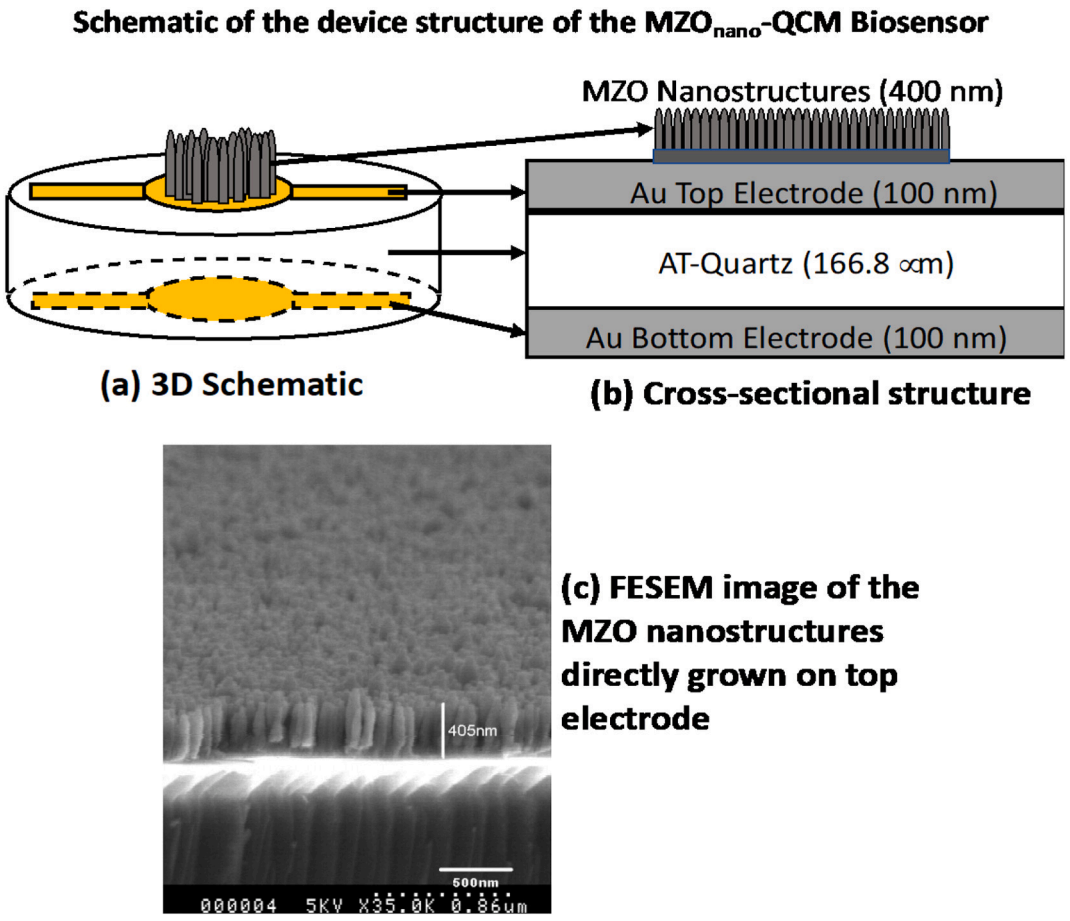


**Fig. 1.** (a) MZO$_{nano}$-QCM sensor device; (b) cross section schematic of the device structure; (c) FESEM image of the MZO nanostructure grown directly on the sensing electrode.

the sensing surface.

### 2.2. Preparation of the bacterial culture

*Staphylococcus epidermidis* ATCC 35984 was inoculated into Tryptic Soy Broth (TSB; Becton Dickinson) and grown at 37 °C for 16–18 h in test tubes placed in a shaking incubator operating at 200 rpm. The resulting stationary phase cultures were diluted 100-fold into fresh TSB medium pre-loaded in the Teflon cell culture well containing the MZO$_{nano}$-QCM. The same 100-fold diluted culture was used in a standard agar plate for colony forming unit (CFU) counting to determine the approximate initial concentration.

### 2.3. Preparation of the antibiotics

We explored the effect of various dosage (concentrations and treatment times) using ciprofloxacin (CIP), oxacillin (OXA), and vancomycin (VAN) as the antibiotic agents for the *S. epidermidis* strain. The antibiotics mentioned above were obtained from the hospitals at the Public Health Research Institute and Department of Microbiology, Biochemistry & Molecular Genetics, New Jersey Medical School, Rutgers University, Newark through the collaboration with Prof. Xilin Zhao. Various concentrations of the drugs were used using dilution with distilled water as the solvent.

### 2.4. Minimum inhibitory concentration (MIC) determination

The minimum inhibitory concentration (MIC) is the lowest concentration of an antibiotic that would cause the disappearance of visible colony growth of the targeted bacteria for a defined period of time. Once the MIC of a particular antibiotic is determined for a specific bacterial culture, this value is taken as the unit of concentration for dosage dependence studies. Thus, in drug susceptibility experiments, the antibiotics introduced into the bacterial culture are expressed in multiples of the MIC value.

The standard laboratory procedure in determining the MIC is the broth microdilution technique (Clinical and Laboratory Standards Institute, 2012; Andrews, 2001). We followed this standard procedure, and describe here the specific details pertinent to our work. Prior to performing the broth microdilution procedure, we determined the *S. epidermidis* growth curve using a standard Klett-Summerson absorption spectrophotometer to measure the turbidity of the cell culture as a function of time to determine the mid-log phase (Brown and Smith, 2017). We prepared the cultures of *S. epidermidis* to grow at mid-log phase based on the growth curve parameters. Cultures of *S. epidermidis* at mid-log phase were then diluted 1:1000 in TSB broth to ~$10^5$ CFU/mL. For each bacterial solution, 50 μL of that solution was dropped in each micro-well of a 96-well plate. Then, 12 different dilutions (successive two-fold dilutions) of the drug is introduced into the a well and incubated at 37 °C for 24 h. The MIC of the drug was determined as the lowest antimicrobial concentration needed to inhibit culture growth, measured by turbidity (using the Klett-Summerson spectrophotometer), by at least 90% relative to an untreated control.

### 2.5. Drug susceptibility determination

Once the MIC of each drug was determined for each of the bacterial strains, we used six different multiples of this MIC value as the set of

antibiotic concentrations for the drug susceptibility determination. For drug susceptibility determination we utilized the standard laboratory method called the soft agar colony formation assay (Brown and Smith, 2017) to count the surviving colonies corresponding to each drug concentration. The results of the colony count from this assay are used as the benchmark with which to compare the results we obtained from the biosensor signals. To perform the standard drug susceptibility assay, we prepared multiple petri dishes coated with 0.25-in.-thick layer of soft agar (Sigma-Aldrich) to serve as the colony formation plates. We prepared a 1:200 diluted overnight bacterial culture (as described in Section 2.2). We distributed this diluted culture into 12 separate incubation flasks. This set of flasks were separated into two groups of six flasks (Batch A and B). Each one of the six flasks from Batch A were treated with antibiotic with concentrations of 0 MIC (no drug), 1 MIC, 2 MIC, 4 MIC, 8 MIC, and 16 MIC respectively. The same antibiotic concentrations were administered to Batch B. The flasks from Batch A were then incubated for 1 h (corresponding to a 1-h dosage) while the ones from Batch B were incubated for 2 h (corresponding to a 2-h dosage).

Once the flasks from Batch A were removed from the incubator after the 1-h incubation period, 10 μL of the culture from each flask was inoculated into a corresponding agar plate. The resulting set of six agar plates will comprise the Batch A colony formation plates. Similarly, the flasks from Batch B were removed from the incubator after the 2-h incubation period and 10 μL of the culture from each flask was inoculated into a corresponding agar plate. Both Batch A and B colony formation plates are then incubated for 15 h.

After the 15-h incubation, all the agar plates were removed from the incubator and inspected for colony formations indicated by small white dots on the agar plate. These colony formations represent bacterial cells that have survived the antibiotic treatments. We determined the total number of surviving colony formation units (CFU) for each drug concentration and incubation time. The percentage ratio of the total surviving CFU over the total CFU without drug treatment was calculated. This ratio represents the survival rate of the bacterial culture for that particular drug concentration and dosage time. The survival rate is then plotted as a function of the multiples of MIC for each dosage time. The family of curves generated from this procedure represent the Drug Susceptibility Curve. This plot signifies the response/susceptibility of the bacterial strain to the drug treatment at various concentrations and dosage times.

### 2.6. Statistical treatment of data

All experiments were performed in three independent trials of similar conditions. The triplicate data were statistically analyzed by taking the average over the three trials and the associated standard deviation. The data points in all plots are the average values over the three trials and the associated error bars are the standard deviation for that data point.

## 3. Results and discussion

### 3.1. Antimicrobial MIC and susceptibility determination from the standard assays

Before we proceed to utilize the $MZO_{nano}$-QCM sensor for drug susceptibility experiments, we first performed the procedures in Sections 2.4 and 2.5 to determine the MIC values for the three antibiotics we are using for *S. epidermidis*. Table 1 shows the result of the MIC determination for the three antibiotics.

Once the MIC values were determined we performed the standard drug susceptibility assay described in Section 2.5 The results for the drug susceptibility assay are shown in Fig. 2(a-c) for the drug response of *S. epidermidis* to CIP, OXA, and VAN antibiotics respectively. These drug response curves will be used in the later sections to compare with the results obtained from the $MZO_{nano}$-QCM for the same bacterial growth and treatment conditions. The drug response curves in Fig. 2(a–c) show that all three antibiotics (CIP, OXA, and VAN) act favorably to the suppression of growth (bacteriostatic effect) and eventual elimination of the *S. epidermidis* bacteria (bacteriocidal effect) in our culture. The plots show that a 1-h dosage of any of the three antibiotics is not enough to cause bactericidal effect unless the concentration of the drug is higher than 15 MIC. On the other hand, we found that bactericidal effect is attained with the 2-h dosage at 10 MIC concentration for all the three antibiotics. Note that these assays (MIC broth dilution and Dynamics assays) are highly labor intensive, very slow (takes up to 1.5 days to complete) and can only report colony formation unit CFU counts and requires large amounts of samples (~30 mL) (Schumacher et al., 2018). Compared to these assays, our technology requires less than 2 mL of samples, involves automatic operation (no user intervention needed), and can report on cell count as well as biophysical transitions of the bacteria during drug treatment.

**Table 1**
Minimum inhibitory concentrations.

| | Ciprofloxacin | Oxacillin | Vancomycin |
|---|---|---|---|
| MIC (μg/mL) | 0.05 | 1.0 | 1.0 |

### 3.2. $MZO_{nano}$-QCM sensor setup and extraction of the motional resistance

#### 3.2.1. Initial sensor setup

In this section we describe the experimental setup to perform dynamic monitoring of *S. epidermidis* growth and response to various antimicrobial treatments using the $MZO_{nano}$-QCM biosensor. Fig. 3(a–b) shows the schematic of the experimental setup. The sensor system is deployed inside a standard cell culture incubator while being connected to an RF signal parameter analyzer. The RF signal parameter analyzer and the sensor are automatically controlled by a data acquisition and microcontroller module (Fig. 3(b)). Two $MZO_{nano}$-QCM sensors are prepared, one serving as control and the other as the test device. These devices are inserted in their accompanying Teflon cell culture containers at the bottom slot and secured with O-rings and screws. Only the sensing area of the $MZO_{nano}$-QCM with the MZO nanostructured coating is exposed in the bottom of the Teflon container. This area will be in direct contact with the bacterial culture. The prototype software program is then initiated to input the following parameters: (i) frequency range of measurement, (ii) desired time interval between measurements, (iii) desired total time of monitoring, and (iv) type of measurement data (frequency shift or acoustic wave transmission spectrum). We then deployed the two containers with sensors inside the incubator with internal temperature of 37 °C. Inside the incubator we connected the sensors to the coaxial cables that interfaces with the signal analyzer and microcontroller and leave the sensors for about 5 min to stabilize their temperature with that of the incubator and take a baseline reading for each sensor. At the current status of our prototype, the analyzer is connected to the sensors with coaxial cables running into the back of the standard incubator. In the future, a wireless circuit will be developed so that no wire is needed to connect the sensors to the analyzer and the data can also be transferred remotely.

#### 3.2.2. Isolate preparation and antibiotic treatment for use in the sensor system

For the selected bacterial isolate, we used the *S. epidermidis* culture prepared using the method described in Section 2.2 and inoculated a specific volume of it to a Klett-Summerson flask with fresh TSB broth and incubated it until it reaches turbidity of 30 Klett Units (optical absorption of 0.15 at 600 nm wavelength) to ensure the isolate bacteria are in the early exponential growth phase. The turbidity was measured using the Klett-Summerson spectrophotometer from Section 2.4. Once

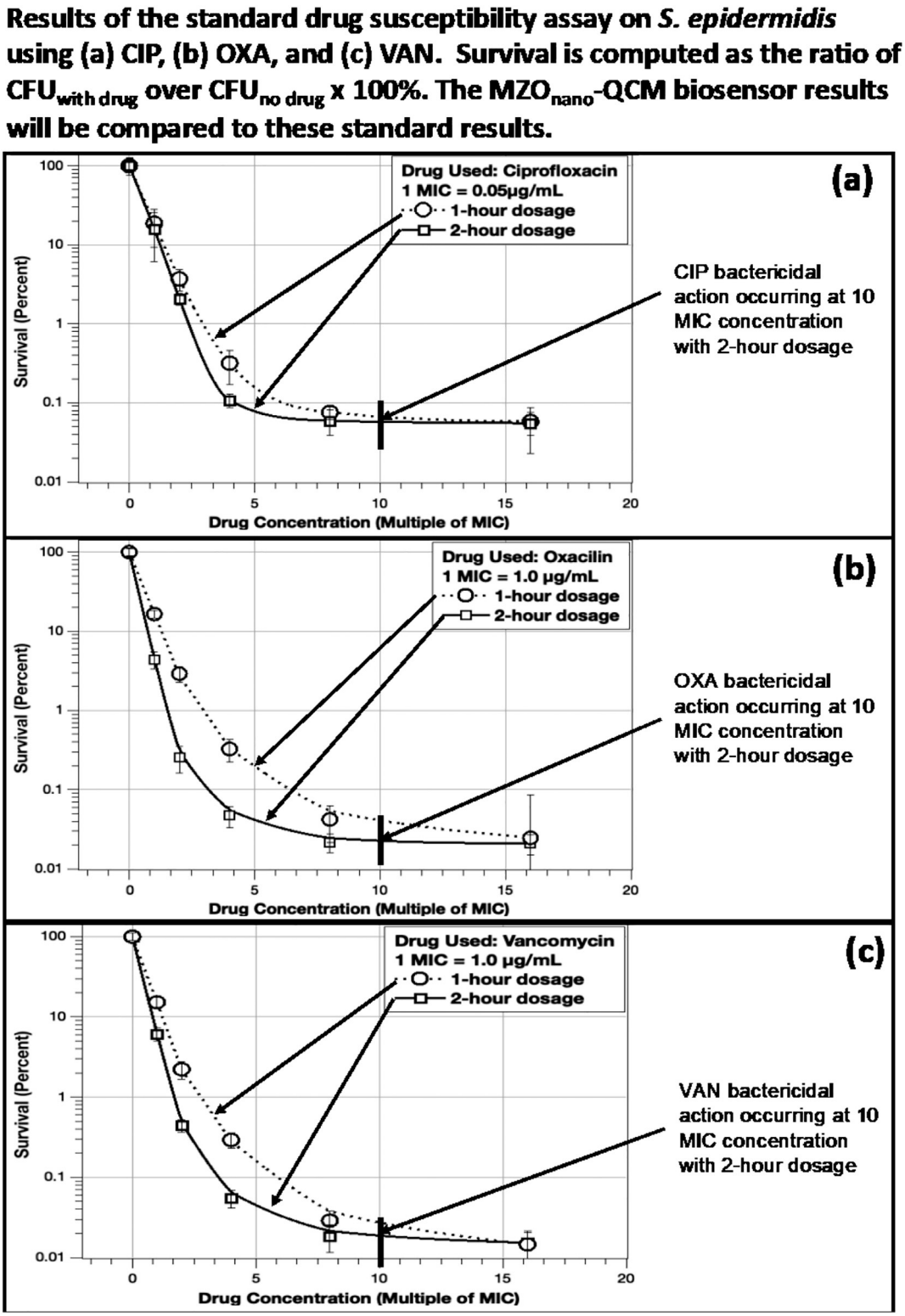


**Fig. 2.** Results of the drug susceptibility assay showing bactericidal action for various drug concentrations (multiples of MIC) and dosage time of (a) CIP, (b) OXA, and (c) VAN for the treatment of *S. epidermidis*.

the isolate solution reaches early exponential growth phase dilute it by 20-fold with pre-warmed (37 °C) TSB medium. We put 2 mL of this solution into both the control sensor and the test sensor that are inside the incubator. Additionally, we administered the drug of specific MIC multiple into the test sensor. The microcontroller is then activated to start the real-time monitoring and signal analysis. Note that no special assay or biomarker preparation is needed to prepare for the sensor. Once the isolates have been prepared in the right dilution, they are ready to be loaded into the sensor. This is one of the major advantages of our work: the sensor requires minimal sample/matrix preparation. This procedure is repeated for each of the three antibiotics in various concentrations. All experiments were done in triplicate. There is no special process needed for diagnostic monitoring and post monitoring.

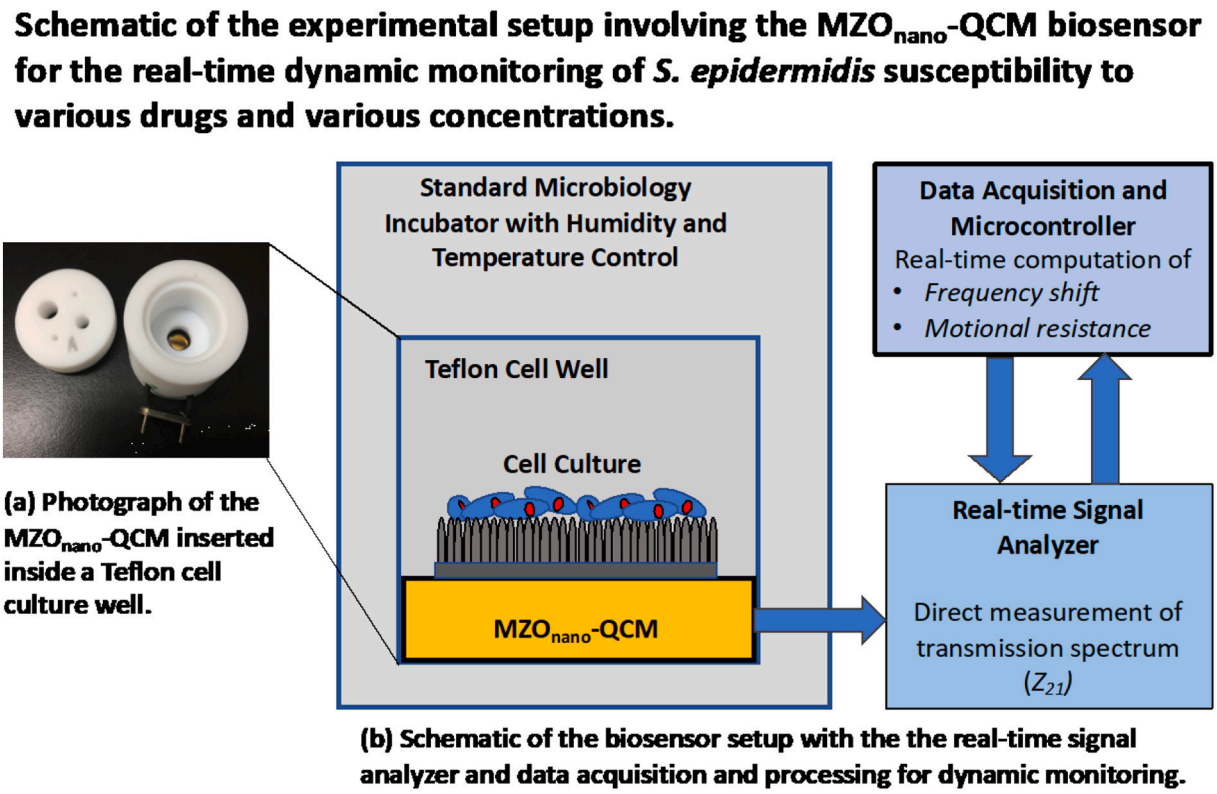


**Fig. 3.** (a) MZO$_{nano}$-QCM sensor device inserted inside the Teflon cell culture well with the active sensing electrode exposed; (b) schematic flow chart of the experimental setup involving the MZO$_{nano}$-QCM sensor-incubator-controller system implemented for this work.

*3.2.3. Extraction and significance of the motional resistance parameter*

The acoustic wave transmission spectrum ($Z_{21}(\omega)$) is the main output signal of the of the MZO$_{nano}$-QCM device. The parameter analyzer and data module from the experimental setup (Fig. 3(b)) perform the automated acquisition and analysis of $Z_{21}(\omega)$ at constant time intervals within the entire duration of the monitoring period. The resulting data is a time series of $Z_{21}(\omega)$. These signals were analyzed by extracting two time-dependent parameters: the shifts in peak frequency and the amplitude modulations. These two parameters give information about the biophysical properties of the cell culture. The peak frequency shifts relative to the starting frequency is attributed to the accumulation of mass on the sensing surface (Sauerbrey, 1959). According to Sauerbrey, the frequency shift of the acoustic wave transmission spectrum is directly proportional to the mass accumulation on the sensing electrode of the QCM by the expression:

$$\frac{\Delta f}{f_0} = \frac{2f_0}{\nu_q \rho_q A}\Delta m \tag{1}$$

where $\Delta f$ is the frequency shift and $f_0$ is the operating frequency of the device, $\nu_q$ and $\rho_q$ are the acoustic velocity and mass density of the AT-cut quartz layer, $A$ is the sensing area of the top electrode, and $\Delta m$ is the accumulated mass on the sensing electrode. The frequency shift as a function of time $\Delta f(t)$ is traditionally the parameter used to describe the temporal behavior of the cell culture being monitored however, we will show later in Section 3.3 that this parameter does not provide a large sensitivity in detection of drug action on the bacterial population.

The spectral amplitude modulations of the MZO$_{nano}$-QCM provide a more accurate and sensitive quantity in characterizing the drug susceptibility of the *S. epidermidis* under drug treatment in the sensor system. From the spectral amplitude modulation, a parameter called the motional resistance can be determined. Under drug treatment, the bacterial cells undergo viscoelastic transitions due to the degradation of the cellular structure due to the drug effects. Using the modified lumped-parameter circuit equivalent called the Butterworth-Van-Dyke (BVD) model (Reyes et al., 2013; Wegener et al., 2000) we can determine a relationship between the motional resistance of the sensor (an acoustic wave quantity) to the mechanical load impedance (a physical quantity) of the accumulated cell culture layer on the MZO nanostructures. According to the BVD equivalent circuit model of the MZO$_{nano}$-QCM, the resulting motional resistance from perturbations contributed by the cell growth layer are related by Eq. (2)

$$R_{Load} = \frac{\pi}{4K^2\omega_0 C_0 Z_{BAW}} \mathrm{Re}\{Z_{mechL}\} \tag{2}$$

where $K^2$ is the coupling coefficient of the piezoelectric layer, $\omega_0$ is the resonant angular frequency of the QCM at no load, $C_0$ is the device capacitance at no load, $Z_{mechL}$ is the mechanical load impedance due to the MZO nanostructure layer + cellular layer + growth medium attached to the basic BAW sensing area at no load ($Z_{BAW}$). From Eq. (2) we can see that the quantity $R_{Load}$ corresponds directly to the mechanical impedance (propensity to resist movement) or motional resistance and designates dissipation of acoustic energy due to the attached cell growth layer on the MZO$_{nano}$-QCM surface. $R_{Load}$ can be extracted easily from the measured data since $R_{Load}$ is just the real part of the acoustic wave transmission spectrum amplitude ($Z_{21}(\omega)$) of the device, i.e. $R_{Load} = \mathrm{Re}\{Z_{21}(\omega)\}$ To eliminate the effects of the surface treated MZO nanostructured layer and the cell growth medium, we separately monitored the impedance transmission spectra of only the nanostructure layer and the growth medium for a period of time. Measurements of both layers have shown no contribution to the dynamic mechanical processes detected by the sensor and can be considered as background signals. After the background signals are subtracted, the output signals correspond solely to cellular activity. In this work, we are using TSB as the growth medium for *S. epidermidis*. TSB has high ionic content and the issue arises on whether this high ionic content might affect the measurement signals. According to (Yang and Thompson, 1993), perturbations to the resonant frequency and

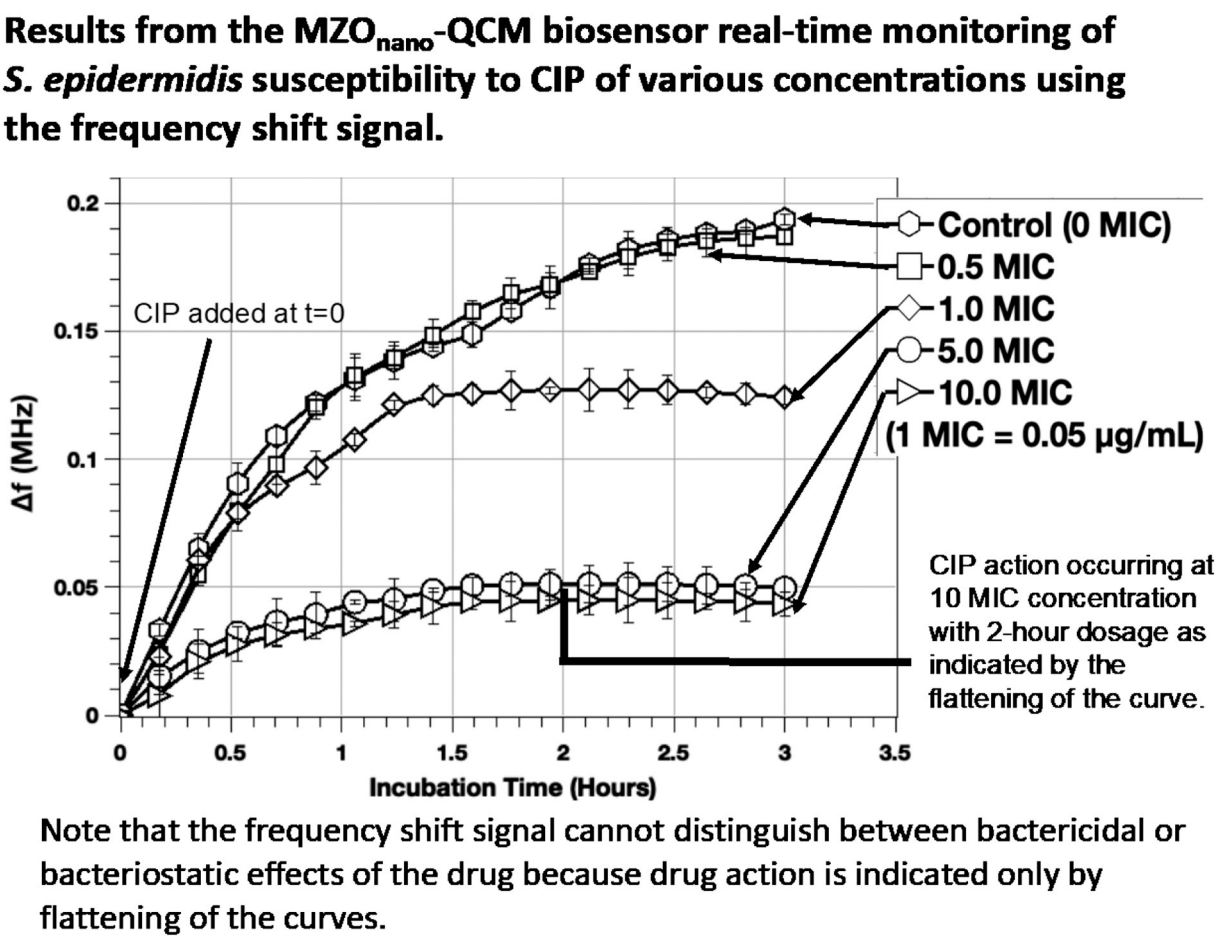


**Fig. 4.** Frequency shift $\Delta f$ plot measured from MZO$_{nano}$-QCM sensor as a function of time for various CIP concentration treatment *S. epidermidis*. (Drug added at $t = 0$, 0 MIC = no drug).

motional impedance are stable in the presence of solutions with high ionic concentrations. This is due to the shielding effect of the electric field at the interface of the electrode and the solution. At low ionic concentrations, an instability in the signal perturbations will be experienced. Therefore, the use of TSB would not introduce signal instability.

### 3.3. Results of dynamic monitoring using MZO$_{nano}$-QCM biosensor

#### 3.3.1. Detection of concentration dependent CIP treatment and comparison of $\Delta f$ and $R_{Load}$ sensitivities

In this subsection we demonstrate the ability of the MZO$_{nano}$-QCM biosensor to dynamically monitor drug susceptibility of *S. epidermidis* to various concentrations of CIP. At the same time, we will compare the sensitivity of the measurement parameters $\Delta f$ and $R_{Load}$. We tested five different MIC multiples of CIP: 0 (no drug), 0.5, 1, 5, and 10. For each concentration value we set a total of 3 h monitoring period with a 10-min interval between measurements. We simultaneously measured $\Delta f$ and $R_{Load}$ of the MZO$_{nano}$-QCM, and compared their temporal plots.

Fig. 4 shows the plot of $\Delta f$ as a function of monitoring time for the five different CIP concentrations. The family of $\Delta f$ curves demonstrate concentration dependent drug susceptibility of *S. epidermidis* to CIP. Time $t = 0$ correspond to the time the drug is introduced into the cell culture. For the no-drug condition (0 MIC), the $\Delta f$ plot increased continuously for the entire duration of the monitoring period, which corresponds to the mass accumulation of the growing bacteria. A similar pattern is observed for the sample that was treated with 0.5 MIC of ciprofloxacin, which indicates that the drug concentration is not enough to kill the bacteria and the population continues to increase and hence increase the mass accumulation on the sensor surface. For the 1 MIC concentration, the plot starts to taper off and flatten after 1.5 h. This result which is expected for the dosage of exactly the minimum inhibitory concentration. However, as the drug concentration introduced to the sample reaches 5 MIC and 10 MIC, the $\Delta f$ vlaue slightly increases up to the 1.5-h point, at which the plot starts to flatten and remain flat until the end of the monitoring period. This trend in the $\Delta f$ plot indicates that for 5 and 10 MIC concentrations of CIP, the *S. epidermidis* population slightly increases but never reaches the same level as the no-drug condition. However, it is not clear from the $\Delta f$ plots whether the effect of the drug at a certain concentration is bacteriostatic or bactericidal. However, we will show that the $R_{Load}$ parameter eliminates this ambiguity by exhibiting a higher sensitivity to transitions in the bacterial culture.

Fig. 5(a) shows the $R_{Load}$ values as a function of incubation time for the same experimental setup. Again, t = 0 correspond to the time the drug is introduced into the bacterial culture. For the case of 0 MIC (no drug), the value of $R_{Load}$ increases continuously until the end of the monitoring period. An increasing value of $R_{Load}$ indicates that there is an increasing number of healthy bacterial cells with high stiffness. Similarly, for the case of 0.5 MIC, $R_{Load}$ increases continuously until the end of the monitoring period, however, at $t = 2$ h and 10 min, the value of $R_{Load}$ slightly declines. For the 1.0 MIC concentration the plot is similar to the no drug case until $t = 1.5$ h where we can see a pronounced change in the graph's profile. The plot changes slope at the 1.5-h monitoring point, then starts decreasing continuously until it tapers off at the 2.5-h point. This shows that the drug has started to take effect and changes the viscoelastic properties of the bacterial cells which is manifested in the sudden decrease in $R_{Load}$. In the case of the 5.0 MIC

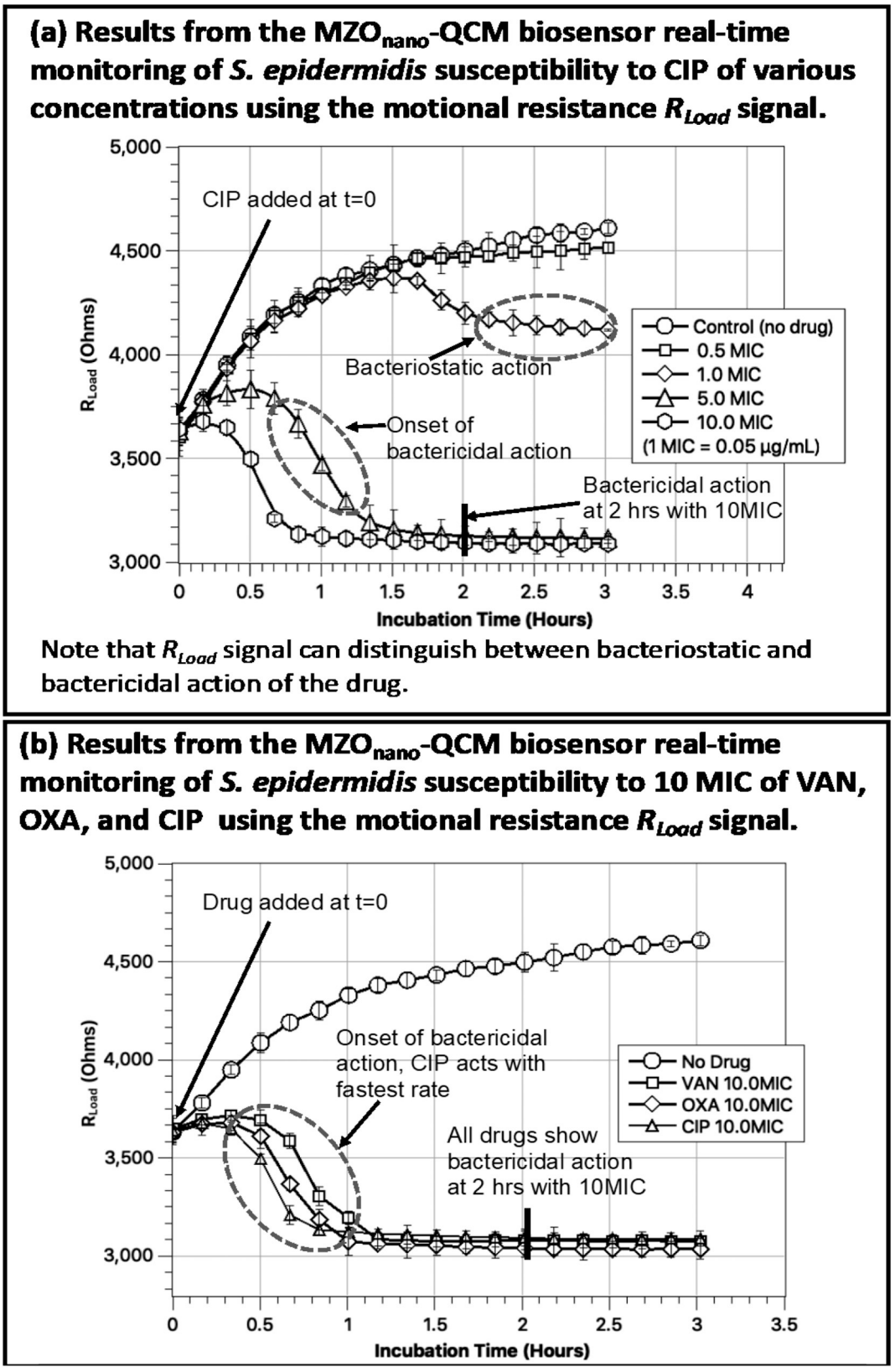


**Fig. 5.** Motional resistance derived from the sensor impedance spectrum as a function of time for (a) various CIP concentrations and (b) various drugs (CIP, OXA, and VAN) on *S. epidermidis*. (Drug added at $t = 0$).

concentration, the $R_{Load}$ plot reaches its peak at the 0.5-h point after which the values of $R_{Load}$ starts to rapidly decline until t = 1.5 h where the plot starts to taper off. Between 0.5 and 1.5 h, the slope reversal and rapid decline in $R_{Load}$ plot indicate the viscoelastic transitions occurring in the bacterial cells as CIP is actively killing the bacteria. After 1.5 h the plot starts to taper off and assume a constant low value until the end of the monitoring period, showing that the bactericidal drug action has successfully taken place. For the 10.0 MIC dosage treatment, the $R_{Load}$ plot shows the similar behavior as in the 5.0 MIC case except the viscoelastic transition region started earlier at around 15 min into the drug treatment and the tapering-off and flatline region started at around 1 h into the treatment.

A comparison of the $\Delta f$ plot in Fig. 4 with the $R_{Load}$ plots in Fig. 5(a) shows that for the same bacterial culture conditions and drug treatment concentrations, the graph profiles of $R_{Load}$ exhibit more pronounced changes or modulations compared to the $\Delta f$ signals. This allows for more accurate extrapolation and determination of the relevant time points in studying the dynamic nature of drug effects on *S. epidermidis*. These two parameters are simultaneously available from the sensor's impedance transmission spectrum signal. The motional resistance complements the information provided by the frequency shift plot and provides higher sensitivity to the sensor.

### 3.3.2. Detection of drug susceptibility to various antibiotics

In this subsection we show the result of utilizing the $MZO_{nano}$-QCM sensor to dynamically monitor the effect of three different antibiotics on *S. epidermidis*. Fig. 5(b) shows the results of the device detecting the effects of 10 MIC concentration of CIP, OXA, and VAN on *S. epidermidis*. The $R_{Load}$ plots from Fig. 5(b) exhibit the same key temporal profiles as in the previous subsection. Fig. 5(b) shows that for all three drugs the viscoelastic transitions of the *S. epidermidis* cells due to the drug effects (indicated by the slope reversal and rapid decline of $R_{Load}$ values) start at around 20 min after the introduction of the drug. The plots start to assume a flat profile at 1 h after the CIP and OXA treatment, and at 1 h and 10 min after the VAN treatment. Also, looking at the rate of decrease of $R_{Load}$ during the transition period, we can see that CIP acts more potently on *S. epidermidis* followed by OXA and then VAN, which is consistent with the results we obtained from the standard drug susceptibility assay in Section 3.1. In addition to the demonstration of dynamic monitoring, we also address the reusability of these compact devices. Because of the high thermal stability of MZO, the device can be autoclaved multiple times without device performance degradation. However, the $MZO_{nano}$-QCM device can be reused for a limited time of up to four successive 3-h monitoring periods after which the MZO nanostructure coating starts to etch off from the top electrode of the QCM device. This may be attributed to the prolonged exposure of the MZO nanostructures to acidic by-products of the bacterial cells during the growth process.

## 4. Conclusion

We developed a magnesium zinc oxide nanostructure modified quartz crystal microbalance biosensor ($MZO_{nano}$-QCM), which consists of a quartz crystal microbalance with MZO nanostructures grown directly on the QCM sensing electrode. The MZO nanostructure surface morphology offers high sensitivity by dramatically increasing the effective surface area available for sensing. The QCM device on the other hand provides dynamic impedance spectrum measurements for real-time sensing. We have established a direct relationship between the mechanical properties of the bacterial cells and the sensor's motional resistance of the device using the $R_{Load}$ parameter. We demonstrated the dynamic and rapid detection of *S. epidermidis* response to various concentrations of CIP and showed that the $R_{Load}$ parameter offers higher sensitivity than the traditional $\Delta f$ signal. We also found that the $R_{Load}$ temporal plot reveals temporal profiles that reveal drug actions at specific monitoring timepoints. We also demonstrated the dynamic monitoring of the response of *S. epidermidis* to various atibiotics (CIP, OXA and VAN) with similar concentrations.

Based on the results achieved in this work, we have demonstrated a promising highly sensitive, dynamic, rapid, compact and low-cost diagnostic sensor that non-invasively monitors bacterial cell behavior for antimicrobial susceptibility. The monitoring procedure is non-invasive, which does not require complicated and labor-intensive pre-analysis preparation that standard assays require and significantly reduces sample volume requirement. The device enables the detection of transitory behavior of bacterial strains during normal growth and dosage dependent drug treatment. This technology could compete as a replacement for the standard labor-intensive MIC assays and resistance testing, including screening antibiotics for activity against resistant strains.

## Acknowledgements

This work is supported by the Rutgers TechAdvance Early Technology Development Fund project number 205719.

## References

Alessandrini, A., Croce, M.A., Tiozzo, R., Facci, P., 2006. Appl. Phys. Lett. 88, 083905.
Andrews, J.M., 2001. J. Antimicrob. Chemother. 48 (Suppl. S1), 5–16.
Anisimkin, V.I., Penza, M., Valentini, A., Quaranta, F., Vasanelli, L., 1995. Sensors Actuators B Chem. 23 (2–3), 197–201.
Atay, S., Pişkin, K., Yılmaz, F., Çakır, C., Yavuz, H., Denizli, A., 2016. Anal. Methods 8, 153–161.
Brown, A.E., Smith, H.R., 2017. Benson's Microbiological applications: Laboratory Manual in General Microbiology. McGraw-Hill Education, 2 Penn Plaza, New York, NY 10121, pp. 140–146.
Chabot, V., Cuerrier, C., Escher, E., AImez, V., Grandois, Charette, P., 2009. Biosens. Bioelectron J. 24, 1667–1673.
Cheng, C., Peng, Y., Bai, J., Zhang, X., Liu, Y., Fan, X., 2014. 2014. Sensors Actuators B Chem. 190, 900–906.
Clinical Laboratory Standards Institute (CLSI), 2012. Methods for Dilution Antimicrobial Susceptibility Tests for Bacteria That Grow Aerobically; Approved Standard—Ninth Edition. CLSI document M07-A9. Clinical and Laboratory Standards Institute, Wayne, PA.
Domingues, M.C., de la Rosa, M., Victoria Borobio, M., 2001. J. Antimicrob. Chemother. 47, 391–398.
Haob, R., Wanga, D., Zhanga, X., Zuob, G., Weia, H., Yang, R., 2009. Biosens. Bioelectron. 24, 1330–1335.
Hsueh, T.-J., Chang, S.-J., Hsu, C.-L., Lin, Y.-R., Chen, I.-C., 2007. Appl. Phys. Lett. 91, 053111.
Hupkes, J., Owen, J.I., Pust, S.E., Bunte, E., 2012. Chem. Phys. Chem. 13, 66–73.
Jorgensen, J., Turnidge, J., 2015. Susceptibility test methods: dilution and disk diffusion methods. In: Jorgensen, J., Pfaller, M., Carroll, K., Funke, G., Landry, M., Richter, S., Warnock, D. (Eds.), Manual of Clinical Microbiology, eleventh ed. ASM Press, Washington, DC, pp. 1253–1273.
Khan, Z.A., Siddiqui, M.F., Park, S., 2019. Current and emerging methods of antibiotic susceptibility testing. Diagnostics 9 (2), 49.
Kleo, K., Schäfer, D., Klar, S., Jacob, D., Grunow, R., 2012. Anal. Bioanal. Chem. 404, 843–851.
Kon, K., Tsukahara, N., Shimomura, M., 2007. Sensors Actuators B Chem. 123 (2), 647–650.
Kon, K., Tsukahara, N., Shimomura, M., 2011. J. Biosci. Bioeng. 111 (2), 242–245.
Ku, C.J., Duan, Z., Reyes, P.I., Lu, Y., Xu, Y., Hsueh, C.L., Garfunkel, E., 2011. Appl. Phys. Lett. 98 (12), 123511.
Kurosawa, S., Park, J.W., Aizawa, H., Wakida, S., Tao, H., Ishihara, K., 2006. Biosens. Bioelecton. 22, 473–481.
Lee, J., Kang, B.S., Hicks, B., Chancellor Jr., T., Chu, B., Wang, W., Keselowsky, Ren, F., Lele, T., 2008. Biomaterials 29, 3743–3749.
Liu, F., Li, Y., Su, X.L., Slavik, M.F., Ying, Y., Wang, J., 2007. Sens. & Instrumen. Food Qual. 1, 161–168.
Mao, X., Yang, L., Su, X.-L., Li, Y., 2006. Biosens. Bioelecton. 21, 1178–1185.
Min, Z., Wei, S., Wu, S., Mian, J., Xue, Y., Zhi, Z., 1984. J. Microbiol. Immunol. Infect. 17 (3), 153–155.
Onodera, A., Tamaki, N., Jin, K., Yamashita, H., 1997. Jpn. J. Appl. Phys. Part I. 36 (9b), 6008.
Park, I.S., Kim, W.Y., Kim, N., 2000. Biosens. Bioelectron. 15, 167–172.
Pirinçci, Ş.Ş., Ertekin, Ö., Laguna, D.E., Özen, F.Ş., Öztürk, Z.Z., Öztürk, S., 2018. Sensors (Basel) 18 (4), 1161.
Reyes, P.I., Zhang, Z., Chen, H., Duan, Z., Zhong, J., Saraf, G., Lu, Y., Taratula, O., Galoppini, E., Boustany, N.N., 2009. IEEE Sensors J. 10 (10), 1302–1307.
Reyes, P.I., Duan, Z., Lu, Y., Khavulya, D., Boustany, N., 2013. Biosens. Bioelectron. 15 (41), 84–89.
Reyes, P.I., Yang, K., Zheng, A., Li, R., Li, G., Lu, Y., Tsang, C.K., Zheng, X.F., 2017. Biosens. Bioelectron. 93, 189–197.

Rodahl, M., Hook, F., Krozer, A., Brzezinski, P., Kasemo, B., 1995. Rev. Sci. Instrum. 66 (7), 3924–3930.
Sauerbrey, G., 1959. Z. Phys. 155, 206.
Schumacher, A., Vranken, T., Malhotra, A., Arts, J.J.C., Habibovic, P., 2018. Eur. J. Clin. Microbiol. Infect. Dis. 37 (2), 187–208. https://doi.org/10.1007/s10096-017-3089-2.
Srikant, V., Sergo, V., Clarke, D.R., 1995. J. Am. Ceram. Soc. 78 (7), 1935.
Su, X.L., Li, Y., 2004. Biosens. Bioelectron. 19, 563–574.
Syal, K., Iriya, R., Yang, Y., Yu, H., Wang, S., Haydel, S.E., Chen, H.Y., Tao, N., 2016. ACS Nano 10 (1), 845–852.
Center for Disease Control and Prevention, 2013. U.S. Department of Health and Human Services. In: Antibiotic Resistance Threats in the United States. https://www.cdc.gov/drugresistance/threat-report-2013/pdf/ar-threats-2013-508.pdf.
Wegener, J., Seebach, J., Janshoff, A., Galla, H.-J., 2000. Biophys. J. 78, 2821–2833.
Wei, A., Sun, X.W., Wang, J.X., Lei, Y., Cai, X.P., Li, C.M., Dong, Z.L., Huang, W., 2006. App. Phys. Lett. 89 (12), 123902.
Yang, M., Thompson, M., 1993. Anal. Chem. 65, 3591–3597.
Zhang, Z., Chen, H., Zhong, J., Saraf, G., Lu, Y., 2007. TMS IEEE J. Electron. Materi. 36 (8), 895.